Volume 24
Number 46
14 December 2022
Pages 8039–8188

CrystEngComm

rsc.li/crystengcomm

ISSN 1466-8033

ROYAL SOCIETY OF CHEMISTRY

PAPER

E. D. Leshchenko and J. Johansson
Interfacial profile of axial nanowire heterostructures in the nucleation limited regime

CrystEngComm

PAPER

View Article Online
View Journal | View Issue

Cite this: *CrystEngComm*, 2022, **24**, 8052

Interfacial profile of axial nanowire heterostructures in the nucleation limited regime

E. D. Leshchenko and J. Johansson *

Received 27th September 2022,
Accepted 11th October 2022

DOI: 10.1039/d2ce01337a

rsc.li/crystengcomm

Heterostructured nanowires exhibit unique physical and electronic properties and are most commonly grown by the vapor–liquid–solid mechanism. Some of these properties are related to the interfacial abruptness of the heterointerface which makes its understanding and control particularly important for further development. In this regard, we present a model based on mass balance of atoms in the catalyst droplet where the atoms incorporate into the solid in the nucleation-limited regime. We explain how and why the decrease of growth temperature and increase of the flux of an element which forms a heterostructure leads to an improvement in the interface abruptness. Our model demonstrates that a sharp heterointerface can be obtained if one uses a high concentration of the foreign catalyst rather than self-catalyzed growth, which can be explained by a reduced reservoir effect. For the examples of InAs/GaAs and GaAs/AlAs heterostructures, we compare the compositional profiles for the two different heterointerface directions.

Introduction

During the last couple of decades, there has been a tremendous interest in semiconductor nanowires,[1–3] which can be explained in the light of the modern paradigm of "materials-on-demand" which implies tailoring the properties to suit the specific requirements. The combination of bottom-up and top-down approaches[4] provides the greatest potential for nanostructured materials: the first one, which is used for conventional nanowire growth enables the control of their crystal structure,[5,6] composition,[7] morphology[5] (both length[8] and radius[9]), and doping,[10] while nanowire density[11] and position[12] can be precisely controlled employing the second, top-down, approach. In addition, the small foot-print of nanowires allows growth on lattice mismatched substrates without the formation of misfit dislocations. As a result, several nanowire-based device prototypes for photovoltaics,[13] optoelectronics[14] and biomedicine[15] have been proposed.

Keeping the fluxes constant, one can growth multicomponent nanostructures with highly isotropic chemical composition. For the majority of materials systems, the nanowire composition can be chosen from the range between two binary compounds AD and BD, where A and B often are group III elements and D is a group V element. Such structures with an intermediate composition x are known as ternary alloys, $A_xB_{1-x}D$.[16,17] If the flux ratio of the same materials group (in this case group III, A/B) is changed during growth, the nanowire composition varies gradually along the growth direction, forming a heterojunction. To produce axial nanowire heterostructures where the junction is along the nanowire[18] one can use the vapor–liquid–solid mechanism[19,20] which involves feeding the liquid catalyst droplet from the vapor phase and, once the droplet is supersaturated, a constantly repeating process of nucleation and growth of monolayers (MLs) occurs at the liquid–solid interface. Growth of radial heterostructures (where the junction is across the nanowire) requires a two-step procedure: vapor–liquid–solid growth of the core and vapor–solid growth of the nanowire shell.[21] However, a spontaneous and often unintended formation of core–shell structures might be observed,[22,23] which has been explained by the growth on the nanowire sidewalls and different precursor decomposition rates close to the droplet and at the sidewalls.

One of the most crucial parameters of heterostructures is the heterojunction abruptness. For the majority of optoelectronic applications, it should be as sharp as possible, ideally, atomically sharp. Fundamentally, the compositional profile depends on the growth method, the growth conditions, and the materials system. However, even if one can instantly switch the composition of the gas phase from A to B precursor, atoms of the A element remain in the catalyst droplet and keep incorporating into the solid leading to the formation of a graded heterojunction. This is the so-called reservoir effect.[24] There are several ways to reduce its effect on the heterojunction abruptness. First, one can use a foreign catalyst, such as gold.[25] The higher the fraction of the foreign catalyst, the less atoms remain in the droplet after

Solid State Physics and NanoLund, Lund University, P O Box 118, SE-221 00 Lund, Sweden. E-mail: jonas.johansson@ftf.lth.se

flux switching. However, atoms of the foreign catalyst might incorporate into the solid contaminating the nanostructure. This is especially crucial for Si-based nanowires.[26] Thus, there is a tendency to use self-catalyzed growth, avoiding the foreign element.[27] Secondly, it is advantageous to grow $IIIV_x$-V_{1-x} heterostructures, since the low solubility of the group V elements guarantees the formation of a sharp interface.[28] Thirdly, heterostructures with abrupt interfaces can be achieved in materials systems with high difference of the chemical potentials of the pure elements. This results in a high incorporation efficiency of one of the components (A or B), even if its concentration in the catalyst droplet is very small. This works well if the heterojunction ends somewhere in the middle range of the chemical composition because the incorporation of the element becomes ineffective at high x and a lot of monolayers are needed to achieve the pure binary compound. For the reverse heterojunction, the beginning of the heterointerface is expected to be very graded (until the solid composition achieves $x \approx 0.1$).[29] Next, low growth temperatures and high desorption rates should provide sharper heterointerfaces. Finally, for the example of the formation of InAs/GaAs heterostructures it has been shown that the interface sharpness can be improved using a pulsed switching technique.[30]

To explain the formation of heterostructured nanowires, various models have been developed by several researchers. The key points here are the description of the liquid–solid incorporation mechanism and the mass balance. In the majority of the theoretical investigations, influxes and outfluxes are described by continuous equations. As for the incorporation into the solid, one of the simplest assumptions is that the growth process occurs at equilibrium. In this case, the compositional profile across a heterostructure can be obtained in the form of a one-parametric equation in terms of the Lambert W function.[31] Another option is the nucleation-limited model where the central part is the formation of the critical nucleus.[32] Its size and composition are defined by the saddle point of the formation energy. The analytical solution has been obtained for materials systems such as AlGaAs, while the InAs/GaAs heterojunction has been studied numerically.[32] An example of the discrete equations, which describe the materials balance and the incorporation rate proportional to the related chemical potentials can be found in ref. 33. The major distinguishing feature of the models that involve the chemical potentials is the presence of the miscibility gap: below certain temperatures, the formation of a homogeneous ternary solution is thermodynamically forbidden inside a certain range of solid compositions.[34]

Instead of thermodynamic considerations, one can consider kinetic ones. Namely, the liquid–solid incorporation rate can be assumed to be proportional to the concentration of the corresponding components in the catalyst droplet.[35] Within such kinetic models all the solid compositions can be achieved. Finally, one can use a Monte-Carlo approach for the description of a heterojunction.[36] It has been shown that for increasing nanowire diameter the heterojunction abruptness decreases in the adsorption-induced growth mode and increases in the diffusion-induced one.

In this investigation, we theoretically investigate the axial heterojunction formation in nanowires grown from a quaternary liquid melt *via* the vapor–liquid–solid mechanism. First, the mass balance for the relevant atoms is introduced. Then, to describe the liquid–solid composition dependence we use a two-component nucleation model. We present analytical solutions for the case of ideal solid solution (zero value of the pseudo-binary interaction parameter) for any heterojunction (such as GaAs/AlAs/GaAs) and for the case of strong interaction between the III–V pairs in the solid for some of the heterojunctions (such as InAs/GaAs). Based on our calculations, we study the effect of the key parameters including temperature, Au concentration, and concentration of group V elements, on the heterointerface. We believe that the results of our investigation promote a deeper understanding of the formation of axial heterostructures in semiconductor nanowires.

Calculations

We consider vapor–liquid–solid growth of a heterostructured nanowire from a droplet which contains a foreign catalyst U (a common example being Au). The self-catalyzed case can be obtained by putting the U concentration to zero. The formation of a nanowire with a BD/AD (for example InAs/GaAs) axial heterojunction occurs as a result of layer-by-layer growth from the liquid catalyst droplet whose chemical composition is changing with time, once the B flux is replaced by the A flux (see Fig. 1). Meanwhile, the droplet becomes quaternary with decreasing concentration of B atoms. Within this intermediate stage an $A_xB_{1-x}D$ ternary solid solution forms where the composition of each layer is defined as $x = N_{AD}/(N_{AD} + N_{BD})$ with N_{AD} and N_{BD} being the numbers of AD and BD pairs in the layer, respectively. We refer to the ratio $y = c_A/(c_A + c_B)$, where c_A and c_B are the atomic fractions of A and B in the liquid, as the liquid composition.

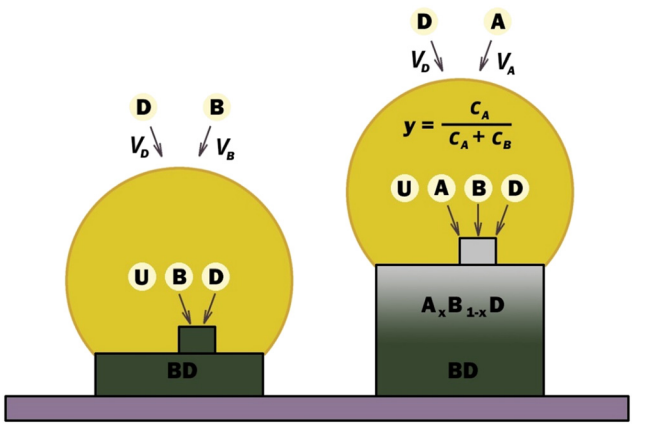

Fig. 1 Schematic illustration of the formation of a nanowire with a BD/AD axial heterostructure.

Assuming the droplet volume doesn't change, the mass balance for the A atoms can be written in the form

$$c_{\mathrm{tot}}\frac{\mathrm{d}y}{\mathrm{d}t}=\frac{V_{\mathrm{A}}}{N_{\mathrm{L}}}-xrg. \tag{1}$$

Here $c_{\mathrm{tot}} = c_{\mathrm{A}} + c_{\mathrm{B}}$, the geometrical coefficient $g = N_{\mathrm{ML}}/N_{\mathrm{L}}$, r is the axial growth rate, N_{L} is the total number of atoms in the liquid phase, N_{ML} is the total number of III–V pairs in a monolayer, and V_{A} is the atomic influx of A elements into the droplet. As can be seen, the number of A atoms increases due to an effective influx (the first term) and decreases as a result of axial nanowire growth (the second term). We now introduce the dimensionless influx of an element which forms a heterostructure $c^{\mathrm{A}} = V_{\mathrm{A}}/(N_{\mathrm{ML}}r)$ and the axial coordinate across the heterointerface $\xi = rt$ (in monolayers). Substituting $\mathrm{d}y/\mathrm{d}t = (\mathrm{d}y/\mathrm{d}x)(\mathrm{d}x/\mathrm{d}t)$, the expression which describes the interfacial abruptness in axial NW heterostructures can be written as

$$\frac{\mathrm{d}\xi}{\mathrm{d}x}=\frac{1}{g}\frac{1}{c^{\mathrm{A}}-x}\frac{\mathrm{d}y}{\mathrm{d}x}c_{\mathrm{tot}}. \tag{2}$$

As can be seen from eqn (2) the liquid–solid composition dependence is needed for further modelling. It relates to the incorporation of atoms from the liquid into the solid which can be described using equilibrium,[31] nucleation,[32,34] or kinetic models.[37–39] The nucleation model describes the formation of the critical nucleus characterized by the chemical composition, x, and size, s. To find them, one should simultaneously maximize the nucleus formation energy F, with respect to s and minimize it with respect to x, that is, solve the system of equations $\partial F/\mathrm{d}x = 0$ and $\partial F/\mathrm{d}s = 0$ to find the saddle point. Ignoring the composition dependence of the nucleus surface energy,[40] the liquid–solid composition dependence in the nucleation-limited regime[34] is given by

$$y=\frac{1}{1+\frac{1-x}{x}\mathrm{e}^{\frac{2\omega_{\mathrm{s}}(x-1/2)+b}{RT}}} \tag{3}$$

with b being a coefficient which depends on the concentrations of all the elements in the liquid particle, the chemical potential differences for the pure components ($\Delta\mu^0_{\mathrm{AD}}$ and $\Delta\mu^0_{\mathrm{BD}}$), and the thermodynamic interaction parameters in the liquid (see ref. 34 for a full definition). Putting $\varepsilon = \mathrm{e}^{b/RT}$, differentiating and substitution into eqn (2) we obtain

$$\frac{\mathrm{d}\xi}{\mathrm{d}x}=\frac{c_{\mathrm{tot}}}{g}\frac{1}{c^{\mathrm{A}}-x}\frac{\varepsilon\mathrm{e}^{2\omega_{\mathrm{s}}(x-1/2)/RT}}{\left(1-\varepsilon\mathrm{e}^{2\omega_{\mathrm{s}}(x-1/2)/RT}\right)^2}\frac{1+2\omega_{\mathrm{s}}x(x-1)/RT}{\left(x+\frac{\varepsilon\mathrm{e}^{2\omega_{\mathrm{s}}(x-1/2)/RT}}{1-\varepsilon\mathrm{e}^{2\omega_{\mathrm{s}}(x-1/2)/RT}}\right)^2}. \tag{4}$$

For heterojunctions in materials systems where $\Delta\mu^0_{\mathrm{AD}} \ll \Delta\mu^0_{\mathrm{BD}}$, $\varepsilon \ll 1$ and simplification and analytical integration of eqn (4) is not possible. However, for the opposite case ($\Delta\mu^0_{\mathrm{AD}} \gg \Delta\mu^0_{\mathrm{BD}}$, resulting in $\varepsilon \gg 1$) eqn (4) can be significantly simplified:

$$\frac{\mathrm{d}\xi}{\mathrm{d}x}=\frac{c_{\mathrm{tot}}}{\varepsilon g}\frac{1}{c^{\mathrm{A}}-x}\frac{1+2\omega_{\mathrm{s}}x(x-1)/RT}{(x-1)^2}\mathrm{e}^{-2\omega_{\mathrm{s}}(x-1/2)/RT}. \tag{5}$$

Partial fraction decomposition and integration of eqn (5) with the initial condition $\xi(x = 0) = 0$ yields the analytic expression

$$\xi=\sum_{l=1}^{3}a_l b_l\left(\ln\left|\frac{n_l}{m_l}\right|-\sum_{i=1}^{\infty}\frac{{n_l}^i-{m_l}^i}{i!i}\left(\frac{2\omega_{\mathrm{s}}}{RT}\right)^i\right) -a_3\left(\frac{\mathrm{e}^{-2\omega_{\mathrm{s}}n_3/RT}}{n_3}-\frac{\mathrm{e}^{-2\omega_{\mathrm{s}}m_3/RT}}{m_3}\right) \tag{6}$$

with the coefficients

$$a_1 = -\frac{c_{\mathrm{tot}}}{\varepsilon g}\frac{1+c^{\mathrm{A}}(c^{\mathrm{A}}-1)2\omega_{\mathrm{s}}/RT}{(c^{\mathrm{A}}-1)^2}\mathrm{e}^{-2\omega_{\mathrm{s}}(c^{\mathrm{A}}-1/2)/RT},$$

$$a_2=\frac{c_{\mathrm{tot}}}{\varepsilon g}\frac{1+(c^{\mathrm{A}}-1)2\omega_{\mathrm{s}}/RT}{(c^{\mathrm{A}}-1)^2}\mathrm{e}^{-\omega_{\mathrm{s}}/RT},$$

$$a_3=\frac{c_{\mathrm{tot}}}{\varepsilon g}\frac{1}{c^{\mathrm{A}}-1}\mathrm{e}^{-\omega_{\mathrm{s}}/RT}. \tag{7}$$

Here $n_1 = x - c^{\mathrm{A}}$ and $n_2 = n_3 = x - 1$, $b_1 = b_2 = 1$ and $b_3 = -2\omega_{\mathrm{s}}/RT$ and $m_1 = -c^{\mathrm{A}}$, $m_2 = m_3 = -1$. eqn (6) consists of seven terms (three logarithms, three infinite series and one exponential expression) and describes the compositional profile across an axial heterostructure in a nanowire when there is a strong interaction of AD and BD pairs in the solid.

For some of the materials systems such as AlGaAs, the pseudobinary interaction parameter is very small and can be ignored. If $\omega_{\mathrm{s}} = 0$, eqn (4) can be reduced to

$$\frac{\mathrm{d}\xi}{\mathrm{d}x}=\frac{c_{\mathrm{tot}}}{g}\frac{\in}{1-\varepsilon}\frac{1}{c^{\mathrm{A}}-x}\frac{1}{(x+\in)^2} \tag{8}$$

with $\in = \varepsilon/(1-\varepsilon)$. Importantly, in contradistinction to ref. 32, this equation can be applied to any heterojunction ($\varepsilon \gg 1$ or $\varepsilon \ll 1$). Obviously, if $\varepsilon \gg 1$, $-\in$ is a number slightly larger than 1, with the immediate consequence that it is difficult to achieve the composition $x = 1$, due to the bracket $(x + \in)^2$ in eqn (8). On the other hand, if $\varepsilon \ll 1$, $x = 1$ can be easily achieved.

The integration of the above equation for BD/AD heterojunction with the initial condition of $\xi(x = 0) = 0$ gives the analytical expression for the compositional profile:

$$\xi=-\frac{c_{\mathrm{tot}}}{g}\frac{\in}{1-\varepsilon}\frac{1}{(\in+c^{\mathrm{A}})^2}\left(\ln\frac{|c^{\mathrm{A}}-x|}{c^{\mathrm{A}}}-\ln\left|\frac{x+\in}{\in}\right|-(\in+c^{\mathrm{A}})\frac{x}{\in(\in+x)}\right). \tag{9}$$

There are two ways to describe the second heterojunction (AD/BD). The calculations might be based on either the mass

balance of B atoms with the constant B flux or a mass balance of the A atoms which remain in the droplet. One should thus be accurate with what x denotes. Keeping our notation where x is the AD concentration in the solid, calculation of the second junction based on the mass balance of B atoms with the initial condition of ($\xi(x = x_{max}) = \xi_{max}$) gives

$$\xi = \xi_{max} - \frac{c_{tot}}{g}\frac{\in}{1-\varepsilon}\frac{1}{\left(\frac{1}{\varepsilon-1}+c^B\right)^2}\left(\ln\left|\frac{1-x-c^B}{1-x_{max}-c^B}\right| - \ln\frac{x+\in}{x_{max}+\in} + \left(\frac{1}{\varepsilon-1}+c^B\right)\frac{x-x_{max}}{(x+\in)(x_{max}+\in)}\right) \quad (10)$$

for AD/BD heterojunction. The mass balance of A atoms with zero flux ($c^A = 0$) gives

$$\xi = \xi_{max} - \frac{c_{tot}}{\varepsilon g}\left(\ln\frac{x}{x_{max}} - \ln\left|\frac{x+\in}{x_{max}+\in}\right| - \in\frac{x-x_{max}}{(x+\in)(x_{max}+\in)}\right) \quad (11)$$

These two different approaches are consistent since $c^B = 1 - c^A$. Thus, there is an interesting case when these two curves coincide, namely if $c^B = 1$ and $c^A = 0$ (or $c^B = 0$ and $c^A = 1$). (see the compositional profile of the second junction in Fig. 5). In such a case the flux of the element (B, or A atoms, respectively) is used to keep the droplet volume constant. When $c < 1$ both A and B fluxes are non-zero. Importantly, the obtained analytical solution can be applied to any materials system and it might be used to describe both AD/BD/AD and BD/AD/BD heterojunctions. As is seen in eqn (6) if $\omega_s = 0$, there are three non-zero terms (two logarithmic terms (l = 1,2) and one exponential term). If $\varepsilon \gg 1$, the analytical solution eqn (6) with $\omega_s = 0$ is the same as eqn (9).

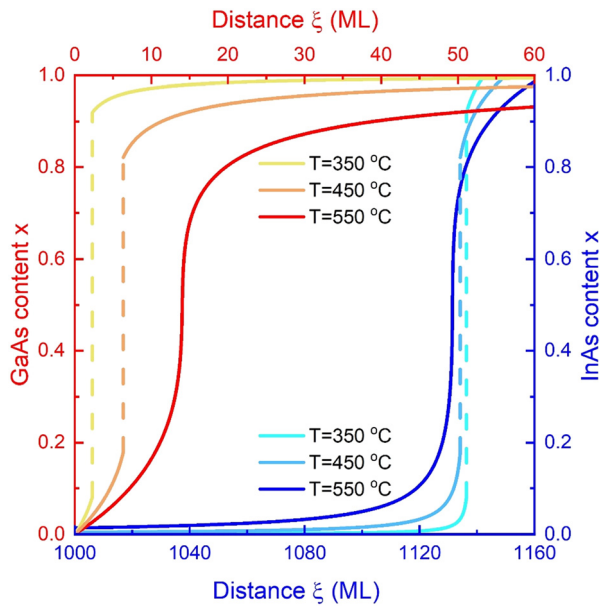

Fig. 2 Composition profiles through InAs/GaAs and GaAs/InAs heterojunctions calculated for self-catalyzed growth at different temperatures. The dashed lines correspond to the miscibility gap.

Results and discussion

We start our analysis with the comparison of the compositional profiles of InAs/GaAs and GaAs/InAs heterojunctions in self-catalyzed nanowires. Fig. 2 shows the dependence of the chemical composition *versus* the coordinate, ξ, along a nanowire at different temperatures and fixed $c_{As} = 0.01$, $c_{Au} = 0$, $c = 1.5$. From here on we use $g = 0.00058$ which corresponds to a nanowire with the radius of 60 nm and the contact angle of 135°. The s-shape of the curves comes from the shape of the liquid–solid composition dependence. The slope of the InAs/GaAs heterojunction before and after the miscibility gap is different: a steep slope at small solid composition ($x < 0.2$) means rapid solid composition change with the axial coordinate across the heterointerface (sharp heterointerface) while a long tail at $x > 0.8$ means that a large number of ternary monolayers is needed to achieve the pure GaAs binary. As can be seen, the interfacial abruptness is much higher for the InAs/GaAs heterojunction (5–20 ML) in comparison with the GaAs/InAs one (~1130 ML). This is because $\Delta\mu^0_{GaAs} \gg \Delta\mu^0_{InAs}$ which results in the necessity of the dominance of one of the components in the droplet (In) to vary the chemical composition in a wide range.[34] Thus, a small amount of Ga atoms in the droplet is needed to start the formation of InAs/GaAs. On the other hand, the formation of the GaAs/InAs heterojunction requires a lot of time (and monolayers), whereas once it reaches the composition of $x \approx 0.1$, 10–40 monolayers (depending on temperature) are needed to achieve pure InAs. Importantly, the GaAs/InAs curve does not coincide with the flipped InAs/GaAs one. For example, 15 monolayers are needed for the path from $x = 0$ to $x = 0.4$ for the InAs/GaAs heterojunction at T = 550 °C, while 30 monolayers are needed for the GaAs/InAs heterojunction with x from 0.6 to 1. As can be seen in Fig. 2, with increasing temperature the interfacial abruptness decreases in both cases. This can be explained by the temperature dependence of the liquid–solid composition curve; it moves closer to $y = x$ and becomes smoother with increasing temperature. In theory, the presence of the miscibility gap (shown by the dashed line in Fig. 2) should provide a high degree of the interfacial abruptness around the miscibility gap. However, there are no experimental observations of the miscibility gap in nanowires. The miscibility gap decreases with increasing temperature because the term $2\omega_s/(RT)$ is also decreases. It should be noted that we use the same value of the flux c = 1.5 for different temperatures. In reality this flux is temperature dependent since the desorption rate and the pyrolysis efficiency (in the case of metalorganic vapor-phase epitaxy) both increase with temperature.

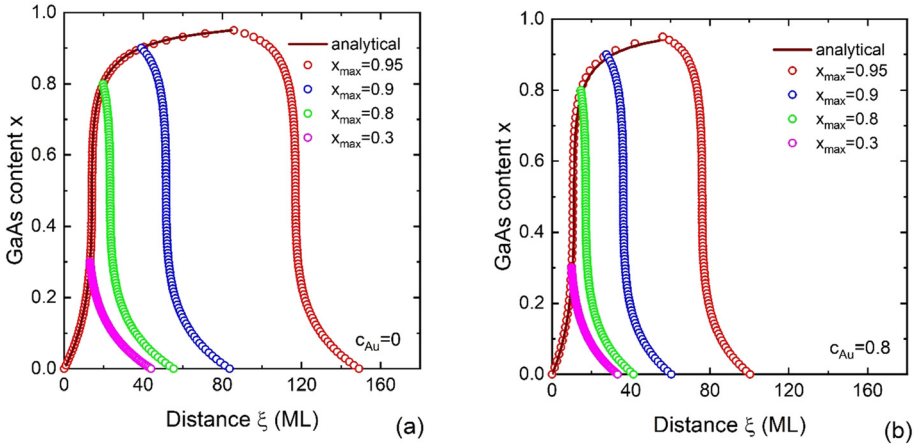

Fig. 3 Numerical and analytical composition profiles through a InAs/InGaAs/InAs double heterostructure calculated for different Au concentrations of c_{Au} = 0 (a) and 0.8 (b).

Next let's consider the influence of the concentration of the foreign catalyst on the interfacial abruptness on the example of an InAs/InGaAs/InAs double heterostructure in Au-catalyzed nanowires. The compositional profiles for Au-catalyzed and self-catalyzed heterostructures are presented in Fig. 3. The parameters used are the following: c_{As} = 0.01, T = 550 °C and c = 1.5. As can be seen, high Au concentration leads to the formation of more abrupt heterojunctions than for self-catalyzed growth. This is due to a reduced reservoir effect which is described by the coefficient c_{tot} in eqn (2). For the double heterostructure InAs/InGaAs/InAs the difference between self-catalyzed and Au-catalyzed growth is significant. For the chosen variables, it is 50 monolayers for x_{max} = 0.95. Fig. 3 also shows the analytical solution, eqn (6), which is based on the assumption that $\varepsilon \approx 88.7$ for c_{Au} = 0 and $\varepsilon \approx 21.4$ for c_{Au} = 0.8. As can be seen, the obtained analytical solution almost coincides with the numerical solution of the initial equation, especially for the self-catalyzed case. We included the first 20 terms in each series while including the first term only in the infinite series leads to a large discrepancy with the numerical solution. From the comparison of the curves calculated at different x_{max}, we conclude that it is not preferable to try to reach pure GaAs but rather to start the second junction with $x \approx 0.8$. This allows one to vary the solid composition in a wide range while the heterointerface remains relatively sharp. Finally, it can be observed that the first and the second junctions are not symmetrical. For all the curves the second junction is always narrower and it is twice as narrow as the first one for x_{max} = 0.95.

Importantly, the description of the first heterojunction is based on the change of the Ga atoms, while the second heterojunction is based on the balance of In atoms. This is in contrast to previous findings[32] where the second junction has been calculated based on the Ga atoms which remain in the droplet. This results in the principial possibility to achieve pure InAs within the second junction which is in contradiction to previous theoretical results.[32] One way of thinking is that the resulting curve consists of two curves taken from Fig. 2 (the curves should be cut and the cyan one should also be flipped across x = 0.5).

Within the nucleation model, the group V element have no effect on the liquid–solid compositional dependence. However, its concentration affects the interfacial abruptness through the growth rate which is considered in the calculations by the coefficient c. Thus, we continue our analysis with the influence of the influx, c, on the heterointerface. Fig. 4 shows the compositional profiles through an InAs/GaAs heterostructured nanowire calculated for different c and at fixed c_{As} = 0.01, T = 550 °C and c_{Au} = 0.5. In order to improve the interfacial abruptness, one should use a high value of c. For example, 35 monolayers are needed to achieve x = 0.8 at c = 1.1, whereas only 5 monolayers are required at c = 5.5. We remind the reader that, c is proportional to the ratio of the atomic flux divided by the elongation rate. Thus, by increasing the atomic flux or by decreasing the growth rate, the droplet composition

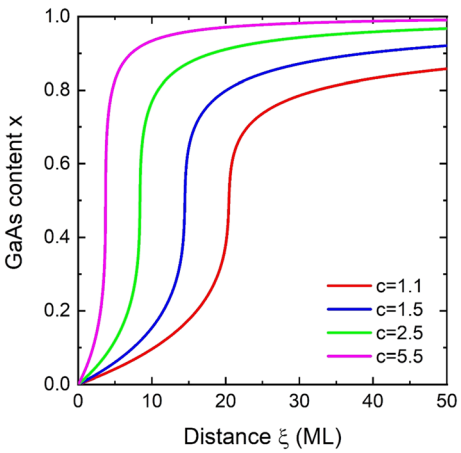

Fig. 4 Composition profiles through an InAs/GaAs heterojunction calculated for different Ga flux, c, at c_{As} = 0.01, T = 550 °C and c_{Au} = 0.5.

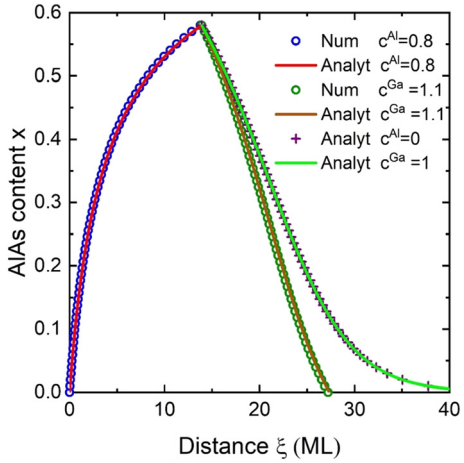

Fig. 5 Composition profiles through the GaAs/AlGaAs/GaAs heterostructure calculated using the Ga and Al atom balance.

changes faster between the nucleation events, which leads to the formation of more abrupt heterojunctions.

The last important case that we will analyse within the nucleation model is the case of a small pseudobinary interaction parameter. In this respect, the compositional profile we consider is the example of the AlGaAs materials system which is widely used in the fabrication of heterostructured nanowires.[31] Comparison of analytical and numerical calculations for the AlAs fraction in a GaAs/AlGaAs/GaAs double heterostructure is presented in Fig. 5. The values used are c_{As} = 0.01, c_{Au} = 0 and T = 610 °C. As can be seen, the numerical and analytical curves coincide. The second junction is calculated using the balance of Ga and Al atoms (the superscript of c denotes the element that c is related to). As has been noticed before, the curves based on Al (plus symbols) and Ga (green curve) coincide if c^{Ga} = 1 and c^{Al} = 0. An increase of the flux results in a more abrupt second junction (compare the green and brown curves). Due to the low pseudobinary interaction parameter there is no miscibililty gap and all the solid compositions can be achieved.

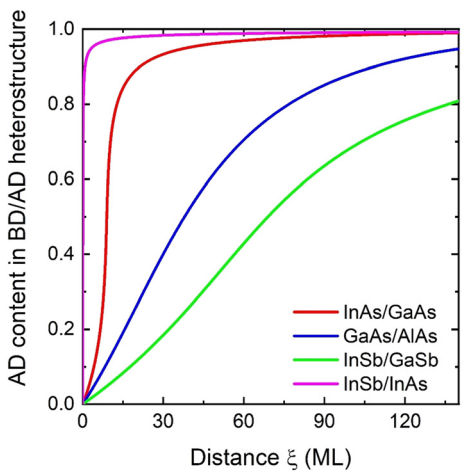

Fig. 6 Composition profiles through the InAs/GaAs, GaAs/AlAs, InSb/GaSb and InSb/InAs heterostructures.

A comparison of heterointerfaces for different materials systems is presented in Fig. 6. For all the calculations the same parameters have been used, namely c_D = 0.02, c_{Au} = 0.5, T = 600 °C, c = 1 for the InSb/InAs heterostructure and c = 3 for the InAs/GaAs, GaAs/AlAs and InSb/GaSb heterostructures. Among the $III_xIII_{1-x}V$ materials systems, the sharpest heterojunction is observed in the InAs/GaAs heterostructured nanowire, while the widest junction corresponds to the InSb/GaSb heterointerface. This is explained by the different values of $\Delta\mu^0_{AD} - \Delta\mu^0_{BD}$. The very sharp heterointerface of only a few monolayers in the InSb/InAs heterostructure can be explained by the reduced reservoir effect. This is a common case in growth of the heterostructured nanowires of $IIIV_xV_{1-x}$ materials systems.[28]

Conclusions

To summarise, we have theoretically studied the formation of axial heterojunctions in vapor–liquid–solid grown III–V nanowires and described the influence of several factors on the interfacial abruptness. The compositional profiles have been discussed in detail within the nucleation-limited model in the examples of the InGaAs materials system (which is a system with high pseudo-binary interaction parameter) and AlGaAs materials system (which is a system with weak pseudo-binary interaction). We have shown that the sharpest heterojunction is formed at low temperature and high flux of the element which forms the heterostructure. We have demonstrated that a heterointerface is sharper in the case of Au-catalyzed growth as compared to the case of self-catalyzed growth, which is attributed to a reduced reservoir effect. Within the nucleation model, the concentration of group V elements has effect on the interfacial abruptness only through the growth rate. Analytical solutions have been presented for the cases of zero and non-zero pseudo-binary interaction parameters. The results coincide with the numerical solution. Our modelling is helpful for understanding the formation of heterostructures and promotes method development towards highly predictable nanowire heterostructure synthesis. An interesting topic for future investigations would be to account for variations of the influx, both due to temperature, but also controlled variations, such as pulsing, which has been utilized in order to get sharper heterointerfaces.

Conflicts of interest

There are no conflicts of interest to declare.

Acknowledgements

LE and JJ acknowledge NanoLund for financial support.

References

1 K. A. Dick, A Review of Nanowire Growth Promoted by Alloys and non-Alloying Elements with Emphasis on Au-Assisted III-V Nanowires, *Prog. Cryst. Growth Charact. Mater.*, 2008, **54**, 138.

2 P. C. McIntyre and A. Fontcuberta i Morral, Semiconductor nanowires: to grow or not to grow?, *Mater. Today Nano*, 2020, **9**, 100058.

3 E. Barrigon, M. Heurlin, Z. X. Bi, B. Monemar and L. Samuelson, Synthesis and Applications of III-V Nanowires, *Chem. Rev.*, 2019, **119**, 9170.

4 A. Wolfsteller, N. Geyer, T. K. Nguyen-Duc, P. Das Anungo, N. D. Zakharov, M. Reiche, W. Erfurth, H. Blumtritt, P. Werner and U. Gosele, Comparison of the top-down and bottom-up approach to fabricate nanowire-based Silicon/Germanium heterostructures, *Thin Solid Films*, 2010, **518**, 2555.

5 K. A. Dick, P. Caroff, J. Bolinsson, M. E. Messing, J. Johansson, K. Deppert, L. R. Wallenberg and L. Samuelson, Control of III-V Nanowire Crystal Structure by Growth Parameter Tuning, *Semicond. Sci. Technol.*, 2010, **25**, 024009.

6 P. Caroff, K. A. Dick, J. Johansson, M. E. Messing, K. Deppert and L. Samuelson, Controlled Polytypic and Twin-Plane Superlattices in III-V Nanowires, *Nat. Nanotechnol.*, 2009, **4**, 50.

7 C. S. Jung, H. S. Kim, G. B. Jung, K. J. Gong, Y. J. Cho, S. Y. Jang, C. H. Kim, C. W. Lee and J. Park, Composition and Phase Tuned InGaAs Alloy Nanowires, *J. Phys. Chem. C*, 2011, **115**, 7843.

8 E. S. Koivusalo, T. V. Hakkarainen, M. D. Guina and V. G. Dubrovskii, Sub-Poissonian Narrowing of Length Distributions Realized in Ga-Catalyzed GaAs Nanowires, *Nano Lett.*, 2017, **17**, 5350.

9 V. G. Dubrovskii, T. Xu, A. D. Alvarez, S. R. Plissard, P. Caroff, F. Glas and B. Grandidier, Self-Equilibration of the Diameter of Ga-Catalyzed GaAs Nanowires, *Nano Lett.*, 2015, **15**, 5580.

10 J. Wallentin and M. T. Borgstrom, Doping of semiconductor nanowires, *J. Mater. Res.*, 2011, **26**, 2142.

11 V. G. Dubrovskii, *Nucleation Theory and Growth of Nanostructures*, Springer, Berlin, Heidelberg, New York, Dordrecht, London, 2014.

12 B. Bauer, A. Rudolph, M. Soda, A. F. I. Morral, J. Zweck, D. Schuh and E. Reiger, Position controlled self-catalyzed growth of GaAs nanowires by molecular beam epitaxy, *Nanotechnology*, 2010, **21**, 435601.

13 M. T. Borgstrom, M. H. Magnusson, F. Dimroth, G. Siefer, O. Hohn, H. Riel, H. Schmid, S. Wirths, M. Bjork, I. Aberg, W. Peijnenburg, M. Vijver, M. Tchernycheva, V. Piazza and L. Samuelson, Towards Nanowire Tandem Junction Solar Cells on Silicon, *IEEE J. Photovolt.*, 2018, **8**, 733.

14 N. Guan, X. Dai, F. H. Julien, J. Eymery, C. Durant and M. Tchernycheva, in *Light-Emitting Diodes, Solid State Lighting Technology and Application Series*, ed. J. Li and G. Zhang, Springer, Cham, 2019, vol. 4.

15 F. Patolsky, G. Zheng and C. M. Lieber, Nanowire Sensors for Medicine and the Life Sciences, *Nanomedicine*, 2006, **1**, 51.

16 M. Ghasemi, E. D. Leshchenko and J. Johansson, Assembling your nanowire: an overview of composition tuning in ternary III-V nanowires, *Nanotechnology*, 2021, **32**, 072001.

17 B. D. Liu, J. Li, W. J. Yang, X. L. Zhang, X. Jiang and Y. Bando, Semiconductor Solid-Solution Nanostructures: Synthesis, Property Tailoring, and Applications, *Small*, 2017, **13**, 1701998.

18 J. Johansson and K. A. Dick, Recent advances in semiconductor nanowire heterostructures, *CrystEngComm*, 2011, **13**, 7175.

19 R. S. Wagner and W. C. Ellis, Vapor-Liquid-Solid Mechanism of Single Crystal Growth, *Appl. Phys. Lett.*, 1964, **4**, 89.

20 E. I. Givargizov, Fundamental Aspects of VLS Growth, *J. Cryst. Growth*, 1975, **31**, 20.

21 M. Royo, M. De Luca, R. Rurali and I. Zardo, A review on III-V core-multishell nanowires: growth, properties, and applications, *J. Phys. D: Appl. Phys.*, 2017, **50**, 143001.

22 W. Sun, Y. Huang, Y. A. Guo, Z. M. Liao, Q. Gao, H. H. Tan, C. Jagadish, X. Z. Liao and J. Zou, Spontaneous formation of core-shell GaAsP nanowires and their enhanced electrical conductivity, *J. Mater. Chem. C*, 2015, **3**, 1745.

23 V. G. Dubrovskii, I. V. Shtrom, R. R. Reznik, Y. B. Samsonenko, A. I. Khrebtov, I. P. Soshnikov, S. Rouvimov, N. Akopian, T. Kasama and G. E. Cirlin, Origin of Spontaneous Core-Shell AlGaAs Nanowires Grown by Molecular Beam Epitaxy, *Cryst. Growth Des.*, 2016, **16**, 7251.

24 N. Li, T. Y. Tan and U. Gösele, Transition region width of nanowire hetero- and pn-junctions grown using vapor-liquid-solid processes, *Appl. Phys. A: Mater. Sci. Process.*, 2008, **90**, 591.

25 M. E. Messing, K. Hillerich, J. Johansson, K. Deppert and K. A. Dick, The use of gold for fabrication of nanowire structures, *Gold Bull.*, 2009, **42**, 172.

26 J. E. Allen, E. R. Hemesath, D. E. Perea, J. L. Lensch-Falk, Z. Y. Li, F. Yin, M. H. Gass, P. Wang, A. L. Bleloch, R. E. Palmer and L. J. Lauhon, High-resolution detection of Au catalyst atoms in Si nanowires, *Nat. Nanotechnol.*, 2008, **3**, 168.

27 A. Fontcuberta i Morral, C. Colombo, G. Abstreiter, J. Arbiol and J. R. Morante, Nucleation mechanism of gallium-assisted molecular beam epitaxy growth of gallium arsenide nanowires, *Appl. Phys. Lett.*, 2008, **92**, 063112.

28 V. Zannier, F. Rossi, V. G. Dubrovskii, D. Ercolani, S. Battiato and L. Sorba, Nanoparticle Stability in Axial InAs-InP Nanowire Heterostructures with Atomically Sharp Interfaces, *Nano Lett.*, 2018, **18**, 167.

29 M. E. Messing, J. Wong-Leung, Z. Zanolli, H. J. Joyce, H. H. Tan, Q. Gao, L. R. Wallenberg, J. Johansson and C. Jagadish, Growth of Straight InAs-on-GaAs Nanowire Heterostructures, *Nano Lett.*, 2011, **11**, 3899.

30 K. A. Dick, J. Bolinsson, B. M. Borg and J. Johansson, Controlling the Abruptness of Axial Heterojunctions in III-V Nanowires: Beyond the Reservoir Effect, *Nano Lett.*, 2012, **12**, 3200.

31 G. Priante, F. Glas, G. Patriarche, K. Pantzas, F. Oehler and J. C. Harmand, Sharpening the Interfaces of Axial Heterostructures in Self-Catalyzed AlGaAs Nanowires: Experiment and Theory, *Nano Lett.*, 2016, **16**, 1917.

32 V. G. Dubrovskii, A. A. Koryakin and N. V. Sibirev, Understanding the composition of ternary III-V nanowires and axial nanowire heterostructures in nucleation-limited regime, *Mater. Des.*, 2017, **132**, 400.

33 P. Periwal, N. V. Sibirev, G. Patriarche, B. Salem, F. Bassani, V. G. Dubrovskii and T. Baron, Composition-Dependent Interfacial Abruptness in Au-Catalyzed Si1-xGex/Si/Si1-xGex Nanowire Heterostructures, *Nano Lett.*, 2014, **14**, 5140.

34 E. D. Leshchenko, M. Ghasemi, V. G. Dubrovskii and J. Johansson, Nucleation-limited composition of ternary III-V nanowires forming from quaternary gold based liquid alloys, *CrystEngComm*, 2018, **20**, 1649.

35 V. G. Dubrovskii and N. V. Sibirev, Factors Influencing the Interfacial Abruptness in Axial III-V Nanowire Heterostructures, *Cryst. Growth Des.*, 2016, **16**, 2019.

36 A. G. Nastovjak, I. G. Neizvestny and N. L. Shwartz, Examination Of Si-Ge Heterostructure Nanowire Growth Using Monte Carlo Simulation, *AIP Conf. Proc.*, 2011, **1399**, 223.

37 J. Johansson and M. Ghasemi, Kinetically limited composition of ternary III-V nanowires, *Phys. Rev. Mater.*, 2017, **1**, 040401(R).

38 E. Roche, Y. Andre, G. Avit, C. Bougerol, D. Castelluci, F. Reveret, E. Gil, F. Medard, J. Leymarie, T. Jean, V. G. Dubrovskii and A. Trassoudaine, Circumventing the miscibility gap in InGaN nanowires emitting from blue to red, *Nanotechnology*, 2018, **29**, 465602.

39 E. D. Leshchenko and J. Johansson, Role of Thermodynamics and Kinetics in the Composition of Ternary III-V Nanowires, *Nanomaterials*, 2020, **10**, 2553.

40 E. D. Leshchenko and J. Johansson, Surface energy driven miscibility gap suppression during nucleation of III-V ternary alloys, *CrystEngComm*, 2021, **23**, 5284.